Supplementary Material

Benchmark scenario and parameters

The VRFB system under consideration is the one developed by Guarnieri and co-workers at Padua University, Italy, as described in a series of papers [18,20]. The geometrical parameters of the stack and the system are those reported in Table 1 while the other material-specific parameters are presented in this section and refer to an operating temperature of 27°C.

The density of positive and negative electrolytes is equal to $\rho_p = \rho_n = 1.350$ kg/L while the viscosities are equal to $\mu_p = 0.007$ Pa·s and $\mu_n = 0.0055$ Pa·s [S.1]. The electrolyte conductivities depend on *SOC*, being equal to $\sigma_p = 41.3 \cdot SOC_p + 27.7 \cdot \left(1 - SOC_p\right)$ and $\sigma_n = 27.5 \cdot SOC_n + 17.5 \cdot \left(1 - SOC_n\right)$ in standard units (S/m) [S.1]. The total concentration of active species is equal to $c_p = c_n = 1.6$ mol/L and the SOC range is constrained between 0.2 and 0.8 if not otherwise specified. According to vanadium electrochemistry, one electron per mole is exchanged at positive and negative electrodes (i.e., $n_p = n_n = 1$) and the standard potential is equal to $E° = 1.37$ V.

The polarisation behaviour of each cell, i.e., the internal resistance r_{in} and limiting current densities $i_{lim,c}$, and $i_{lim,d}$, is fitted from experimental data for different *SOCs* and area-specific flowrates q. Two examples of which, coming from Compbat project deliverable 3.1 [S.2], are reported in Figure S.1, where positive and negative values of current density indicate discharge and charge operations, respectively. As already anticipated, the linearization of the polarization curve as detailed in Section 2.2 introduces only a minimal error in the $\varphi(i,SOC,q)$ function, being able to take into account, in a nutshell, all the electrochemical losses taking place inside the cell due to reaction kinetics, mass transport resistance, membrane and bipolar plate ohmic drops. Finally, crossover losses are accounted for according to the crossover flux expression described in Eq. (13) in Section 2.3.

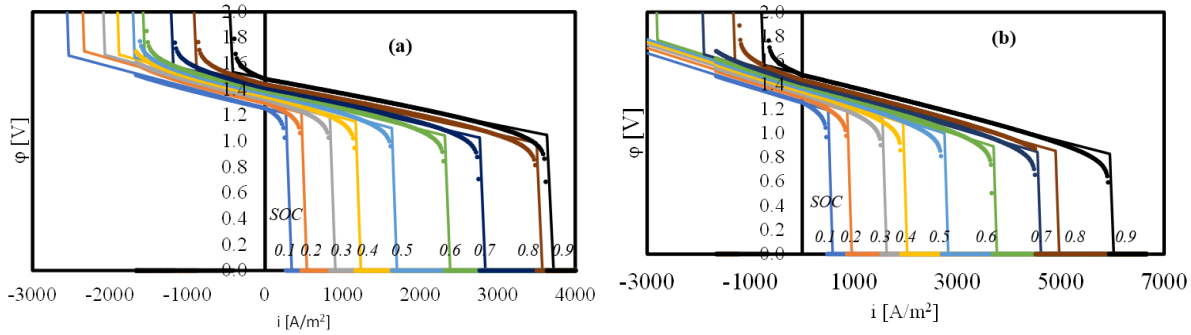


Figure S1. Polarisation behaviour of a single cell in the VRFB system for different *SOCs* at (a) $Q = 10$ L/min (i.e., $q = 6.94 \cdot 10^{-5}$ m³/(m²s)) (b) $Q = 20$ L/min (i.e., $q = 1.39 \cdot 10^{-4}$ m³/(m²s)) from experimental data (symbols) and linear fit (solid lines).

Resistor Network

The hydraulic circuit of the stack, depicted in Figure 1, can be effectively reduced to a resistor network, for shunt currents evaluation. Figure S.2 shows the details of the derivation of the resistor network model, some simplifying assumptions are made to reduce the network complexity by exploiting the symmetry between input and output sides. In particular, it is assumed the geometries of the inlet and outlet sides of the stack are identical and that the electrolyte conductivity σ does not change significantly between inlet and outlet upon a change in *SOC*. Under these assumptions, which are satisfied in all the conditions considered in this work, the network can be simplified as shown in Figure S.2, accounting for the ohmic resistances of manifolds (R_M^{eq}) and of feeding ports and cells (R_{FC}^{eq}) for both the positive and negative sides, calculated according to Ohm law.

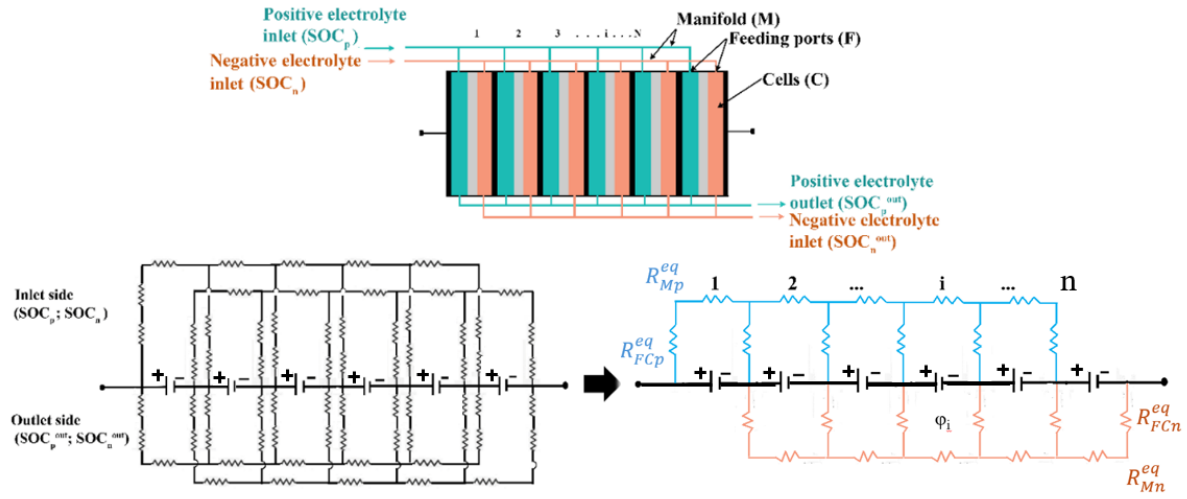


Figure S2. RFB scheme and resistor network arrangement for the evaluation of shunt currents.

Figure S.3 shows how the *i*-th cell in the stack can be represented as an equivalent circuit; L_C, L_F, and L_M denote the length of the cell, feeding port, and manifolds of the internal hydraulic circuit within the stack, wherein electrolyte flows. By considering the centre of the cell as a reference plane, each length can be associated with an ohmic resistance, namely R_C, R_F, and R_M, respectively, where the electrolyte properties are those at the stack inlet (superscript *in*) or stack outlet (superscript *out*). Both compartments, i.e., positive, and negative, must be considered.

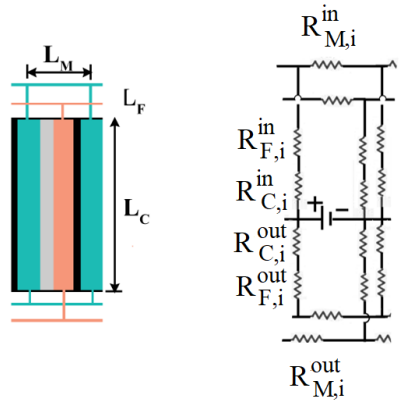


Figure S3. Geometrical representation of the *i*-th cell in RFB stack and its resistor network analogue.

The resistances of cell, feeding port, and manifold are evaluated according to Ohm law as in Eqs. (S.1)-(S.3) by considering their length and cross section area (A_C, A_F, A_M, respectively), along with the ionic conductivity σ of the electrolyte, which is corrected by the effective conductivity factor ε in the cell since the electrodes are porous:

$$R_M = \frac{L_M}{\sigma}\frac{1}{A_M} \tag{S.1}$$

$$R_F = \frac{L_F}{\sigma}\frac{1}{A_F} \tag{S.2}$$

$$R_C = \frac{L_C/2}{\varepsilon\cdot\sigma}\cdot\frac{1}{A_C} \tag{S.3}$$

The resistances are calculated for both the positive and negative compartments at the inlet and outlet according to the electrolyte conductivity σ, which can vary with the *SOC*.

By assuming that the geometry of the stack is identically, symmetric between the inlet and outlet, sides and that the *SOC* difference between inlet and outlet is sufficiently small, so that the electrolyte conductivity σ is rather constant in the stack. Hence, the symmetry of the network can be exploited to simplify it with equivalent resistances of parallel pairs as reported in Eq. (S.4) and shown in Figure S.4 for both positive and negative sides. Finally, the equivalent feed and cell resistances are in series, thus can be summed up as in Eq. (S.5).

$$R_j^{eq} = \frac{1}{2}R_j \qquad \text{for } j = M, F, C \tag{S.4}$$

$$R_{FC}^{eq} = R_F^{eq} + R_C^{eq} \tag{S.5}$$

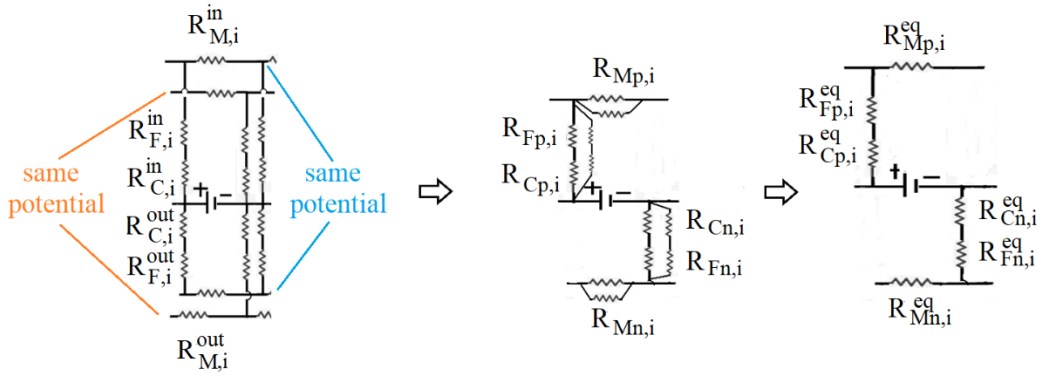


Figure S4. Exploiting symmetry to simplify the network.

Finally, since the *SOC* difference between inlet and outlet is assumed to be small, a single value of electrolyte conductivity, calculated at the inlet *SOC*, can be considered. Then, since the geometry of the cells is the same along with the stack, there is no need to determine the equivalent resistances for each cell *i*, so that only four values of equivalent resistances are required, namely R_{Mp}^{eq}, R_{FCp}^{eq}, R_{Mn}^{eq}, and R_{FCn}^{eq} as shown in Figure S.5, which reports the final resistor network.

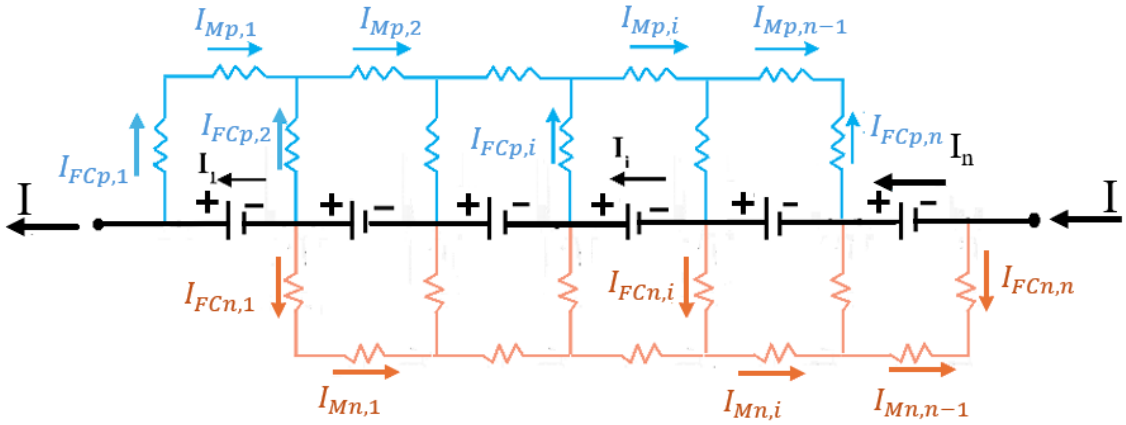


Figure S5. Final resistor network with equivalent resistances.

To evaluate the currents in the whole stack, both the parasitic ones ($I_{Mp,i}$, $I_{FCp,i}$, $I_{Mn,i}$, $I_{FCn,i}$) and those circulating within each cell (I_i) as labelled on the left in Figure S.6, Kirchhoff laws are used to solve a linear system of algebraic equations. In particular, taking as a reference the *i*-th cell on the right of Figure S.6, 5 equations can be written to solve for the 5 unknowns $I_{FCp,i}$, $I_{Mp,i}$, I_i, $I_{FCm,i}$, $I_{Mm,i}$. Thus, for each cell the following linear system needs to be solved:

$$
\begin{cases}
\text{on point } P_i : I_{Mp,i-1} + I_{FCp,i} - I_{Mp,i} = 0 \\
\text{on point } C_i : -I_{i-1} + I_i - I_{FCp,i} - I_{FCn,i-1} = 0 \\
\text{on point } N_i : I_{Mn,i-1} + I_{FCn,i} - I_{Mn,i} = 0 \\
\text{on loop } L_{n,i} : -\varphi_i + R_{FCn} \cdot I_{FCn,i-1} + R_{Mn} \cdot I_{Mn,i-1} - R_{FCn} I_{FCn,i} = 0 \\
\text{on loop } L_{p,i-1} : +\varphi_{i-1} + R_{FCp} \cdot I_{FCp,i} - R_{Mp} \cdot I_{Mp,i-1} - R_{FCp} I_{FCp,i-1} = 0
\end{cases}
$$

For the sake of completeness, equations for cells *1* and *N* require a little modification due to the absence of two variables.

It should be stressed that the cell potentials φ_i are a function of the current I_i and *SOC* and flowrate *Q*, thus making the problem non-linear and dynamic. Thus, the resistor network is solved in COMSOL Multiphysics along with the other model equations reported in paper Section 2.

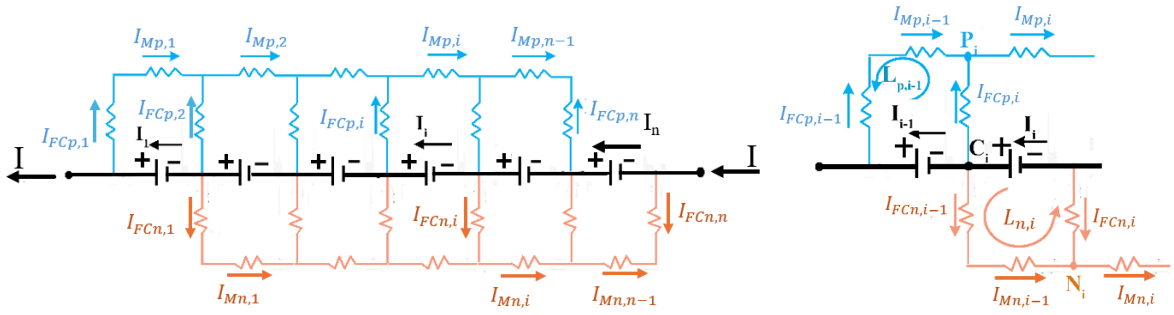


Figure S6. Current direction in cell stack and Kirchhoff laws for current distribution applied to the *i*-th cell.

Pumping losses

Here the details are presented about how the pumping losses have been evaluated and how the respective energy consumption has been estimated, starting from the dependency between circuit pressure drop and electrolyte volumetric flow, see Figure S.7, measured in [18].

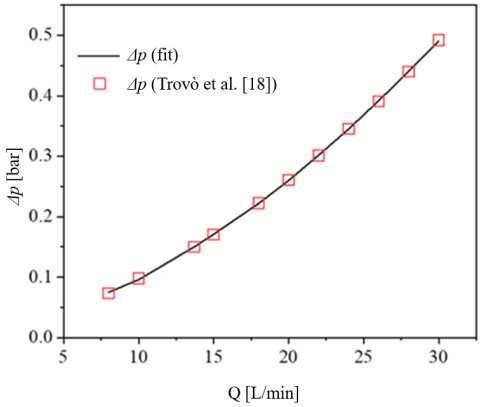


Figure S7. Pressure drop data of the 40-cells stack considered by Trovò et al. [18] for the negative electrolyte of VRFB at *SOC* = 50%, for which μ = 0.055 Pa·s and ρ = 1350 kg/m^3.

The pumping AC electric power losses (P_{pu}) are then evaluated by calculating the hydraulic power needed to circulate the electrolyte through the whole system, which is the product of pressure drop Δp and volumetric flowrate Q, and dividing it by the hydraulic efficiency of the pump needed to identify the mechanical power it needs from the pump (η_{hy}, evaluated as a function of Q as in Figure S.8), then divided by the electric motor efficiency to calculate the DC electric power (η_{mo}, equal to 50% [18]), and finally by the inverter (η_{in}, equal to 95% [18]) for both the positive and negative sides of the system, each with its pump, motor and inverter:

$$P_{pu} = (\Delta p_p Q_p)/(\eta_{hy}\eta_{mo}\eta_{im,p}) + (\Delta p_n Q_n)/(\eta_{hy}\eta_{mo}\eta_{im,n}) \quad \text{(S.6)}$$

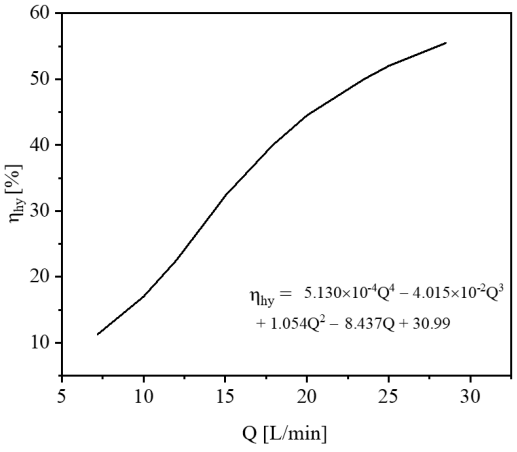


Figure S8. Pump hydraulic efficiency η_{hy} as a function of flowrate as reported by Trovò et al. [18], along with the interpolating function used in this report.

The validity of Eqs. (14) and (S.6) are corroborated by comparing, Fig. S.9, the calculated hydraulic power losses with the data reported in the literature for a 40-cells VRFB system at *SOC* = 50% [18]: the series in blue report the mechanical power loss due to the circuit hydraulic frictions ($\Delta p \cdot Q$) while the series in red report the overall AC electric pumping losses; the difference between the two series is due to the hydraulic efficiency of the pump, the efficiencies of the motor and inverter.

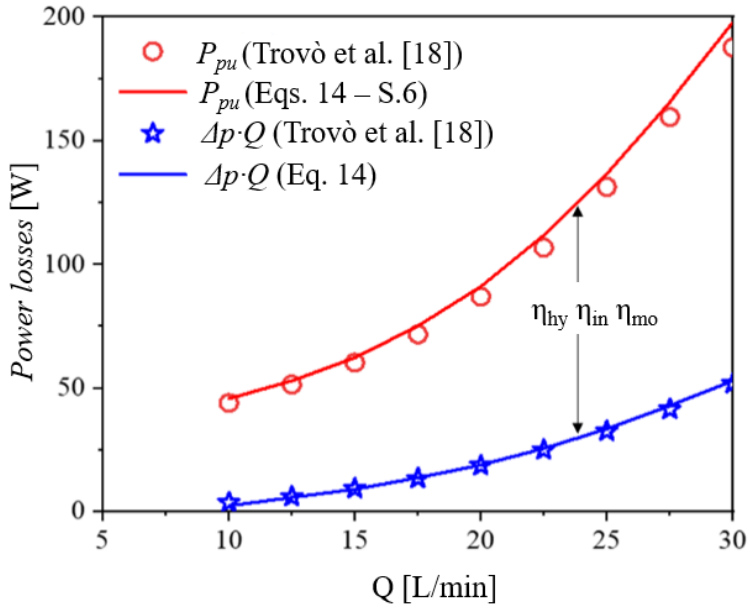


Figure S9. Pumping power losses as a function of flow rate at *SOC* = 50% in both positive and negative compartments for the 40-cells stack VRFB system investigated by Trovò et al. [18].

The positive comparison between the values calculated via Eqs. (14) and (S.6) and those reported in the experimental study [18] indicate that pumping losses are determined with sufficient accuracy for the 40-cells stack system under consideration. It should be stressed that the hydraulic and motor efficiencies happen to be low due to the intrinsically small size of the pumps, i.e., about 100 W, which is the typical pump size for a domestic application of a few kW redox flow battery. For larger sizes, a significant increase in hydraulic and electric motor efficiencies is expected.

Reference

S.1. Choi, C.; Kim, S.; Kim, R.; Choi, Y.; Kim, S.; Jung, H.; Yang, J.; Kim, H. A review of vanadium electrolytes for vanadium redox flow batteries. *Renewable and Sustainable Energy Reviews* **2017**, *69*, 263–274.

S.2. Stevenson, K.; Pugach, M.; Kurilovich, A.; Ryzhov, A.; Gonzalez, G. Deliverable 3.1: Report on general isothermal cell modelling, *Computer aided design for next generation flow batteries (CompBat) Project, Grant agreement ID: 875565*, **2021**.